CHINESE OPTICS LETTERS

Vol. 20, No. 3 | March 2022

Secondary structure changes of ox-LDL by photoirradiation in an optofluidic resonator

Yuxi Shang (尚宇晞)[1], Hailang Dai (戴海浪)[1*], Daopeng Dai (戴道鹏)[2], Jinmao Gu (顾进茂)[3], Meng Zhang (张 萌)[1], Qiheng Wei (魏麒恒)[1], and Xianfeng Chen (陈险峰)[1,4,5,6**]

[1] State Key Laboratory of Advanced Optical Communication Systems and Networks, School of Physics and Astronomy, Shanghai Jiao Tong University, Shanghai 200240, China

[2] Department of Cardiology, Ruijin Hospital, Shanghai Jiao Tong University School of Medicine, Shanghai 200240, China

[3] The Affiliated Hospital of Tianjin Chinese Medical Institute, Tongji University, Shanghai 200092, China

[4] Shanghai Research Center for Quantum Sciences, Shanghai 201315, China

[5] Jinan Institute of Quantum Technology, Jinan 250101, China

[6] Collaborative Innovation Center of Light Manipulation and Applications, Shandong Normal University, Jinan 250358, China

*Corresponding author: hailangdai@sjtu.edu.cn

**Corresponding author: xfchen@sjtu.edu.cn

Received November 1, 2021 | Accepted December 29, 2021 | Posted Online January 24, 2022

Atherosclerotic cardio-cerebral vascular disease is the most common disease that threatens human health. Many researches indicated that oxidatively modified low-density lipoprotein (ox-LDL) is a key pathogenic factor of atherosclerosis. Here, we report the change of the secondary structure of ox-LDL caused by photoirradiation in an optofluidic resonator. The content ratios of amphipathic α-helices and β-sheets of ox-LDL are changed under laser beam illumination, resulting in an increasing binding rate of ox-LDL and ox-LDL antibodies. Our findings may provide a potential way for clinical atherosclerosis treatment and prompt recovery rate of atherosclerotic cardio-cerebral vascular disease by optical technology and immunotherapy.

Keywords: atherosclerosis; ox-LDL; optofluidic resonator; photoirradiation.
DOI: 10.3788/COL202220.031702

1. Introduction

Cardiovascular disease is the leading killer of human beings during the past two decades. About two million people died from cardiovascular disease in 2019, constituting 16% of all global deaths (from the World Health Organization, 2020). Therein, atherosclerosis is one of the direct causes of various cardiovascular diseases[1–3]. Atherosclerosis plaque, which is present along the arteries, is caused by fatty deposits. With the plaque formation, the arterial walls will thicken, and blood flow will be blocked, which causes high blood pressure. Eventually, the ruptured plaque leads to atherothrombosis, coronary heart disease, insufficient oxygen, and nutrient delivery to the end organs. Based on previous studies, the low-density lipoprotein (LDL) is a significant risk factor of the atherosclerosis plaque genesis. Meanwhile, oxidized LDL (ox-LDL) is the key determining pathogenic factor of vascular atherosclerosis and plays a more harmful role in the initiation and progression of atherosclerosis than LDL[4–8]. Furthermore, ox-LDL is throughout all stages of the atherosclerosis process, including inducing endothelial cell apoptosis[9], promoting foam cells and thrombosis[10–13], and accelerating atherosclerosis plaques rupturing[14–16]. Many clinical studies reported that an elevated level of ox-LDL in blood is the criteria that can diagnose patients with cardiovascular disease[17]. Therefore, ox-LDL is a specific biomarker in atherosclerosis diagnosis and treatment. The normal detection method of ox-LDL is enzyme-linked immunosorbent assay (ELISA) based on a variety of antibodies, such as 4E6, E06, and DLH3[18]. Recently, there are many new methods to detect ox-LDL from blood, such as the fluorescence probe technique[19], capillary electrophoresis[20,21], and gold nanoparticle conjugation[22,23]. However, the majority of researches are devoted to the pathogenicity mechanism and detection methods of ox-LDL, which focus on the properties of ox-LDL and indirect treatment support of atherosclerosis. Because exceeding ox-LDL is removed by effective and simple ways to treat atherosclerosis directly, treatment has been focused on and sought in the medical and interdisciplinary fields.

In this paper, we demonstrate a new way to study ox-LDL by optical technology, which can change the secondary structure of ox-LDL by laser irradiation in an optofluidic resonator. The optofluidic resonator is a hollow-core metal-cladding waveguide (HCMW) constituted by three layers of slab glass. Based on free space coupling technology[2] and cavity mode resonance, the density of light in the HCMW can be enhanced and reach a large value with a low-power incident laser. After low-power continuous-wave (CW) laser irradiation, the content ratio of the α-helix and β-sheet of ox-LDL are changed, which promotes ox-LDL antigen-antibody binding. Meanwhile, the cause of ox-LDL secondary structure variation has been elucidated, and the parameters in the irradiation experiment have been discussed, which may pave a new way for clinical atherosclerosis treatment.

2. Materials and Methods

2.1. Experimental setup

The experimental setup (Fig. S3 in Supplementary Materials) consists of a CW laser (532 nm, 100 mW, MSL-FN-532, Changchun New Industries Optoelectronics Technology Co., Ltd., Changchun, China), an optical attenuator, two apertures, a synchronous rotator, a photoelectric detector, and an HCMW. The 532 nm laser beam was collimated by two apertures, and then an optical attenuator modulated the laser beam intensity. The HCMW filled with ox-LDL was illuminated for a time, and the intensity of reflected light was measured and recorded by a photoelectric detector.

The HCMW is a kind of optofluidic resonator, and the schematic of the structure is shown in Fig. 1(a). It includes five parts, and three layers in the middle constitute a 1 mm thick glass slab cavity. The top and bottom surfaces of the glass slab cavity are parallel (less than 4 in.). The upper silver film (about 35 nm thick) can couple the incident light into the HCMW. Another 300 nm thick silver film is utilized for a substrate layer in the bottom. The silver layers were fabricated by vacuum evaporation technology. After ultrasonic cleaning, the HCMW was coated with 300 nm Ag film on the bottom surface and 30 nm Ag film on the top surface in a vacuum evaporator (Beijing Technol Science Co., Ltd., Beijing, China). The Ag pellets were purchased from ZhongNuo Advanced Material Technology Co., Ltd. (Beijing, China). The purity of the Ag pellet is higher than 99.99%. The length and diameter of the Ag pellet are 5 mm and 2 mm, respectively. To prevent the Ag from evaporating into the cavity, both sides of the cavity should be covered during the vacuum evaporation.

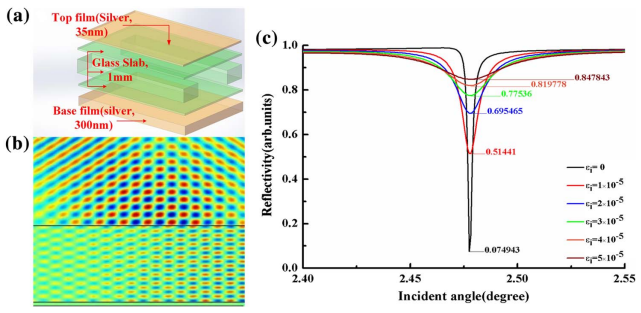

Fig. 1. Structure and properties of the HCMW. (a) HCMW 3D schematic diagram. (b) The COMSOL simulation image of the HCMW. (c) The reflectivity simulation image of the HCMW with different imaginary parts of dielectric coefficient ε_i (from 0 to 1×10^5).

Due to the thin metal coupling layer and the small effective refractive index, the incident light can be coupled from the free space into the guiding layer without any additional coupler such as a grating or high-index prism[24,25]. Figure 1(b) shows the COMSOL simulation electromagnetic field distribution of the HCMW. The standing optical field oscillates rapidly between the coupling layer and substrate layer, which results in many properties such as strong field enhancement and high sensitivity[26]. Because of the symmetrical metal cladding, the incident light can be trapped in the HCMW, which is filled with the low refractive index liquid, so that the light and matter can interact sufficiently. The high-density cavity modes in the HCMW can be recorded, which are highly sensitive with fast responsivity to detect the change of content's refractive index in the cavity. The attenuated total reflection (ATR) simulation spectra of the reflectivity change due to different dielectric coefficients with the same incident angle are presented in Fig. 1(c). When the dielectric coefficient of the liquid in cavity increases by 1×10^5, the reflectivity of the HCMW increases significantly. As we know, the imaginary part of the refractive index represents the absorbance of light, and the secondary structure of the bio-molecule change would result in the absorbance change of the incident light. Thus, HCMW can not only form a strong field to induce the change of ox-LDL's secondary structure under the light illumination, but also detect the change of the content's refractive index in the cavity in real time.

Human ox-LDL used in experiments was purchased from Dalian Meilun Biotech Co., Ltd. (Dalian, China). The purity of ox-LDL is more than 98%, and the concentration of ox-LDL is 2.2 mg/mL. There are traces of phosphate buffered saline (PBS) and ethylenediaminetetraacetic acid (EDTA)-Na2 in ox-LDL. Ox-LDL and LDL are key risk factors for the genesis of atherosclerosis plaque, they can transport cholesterol, and ox-LDL-cholesterol migrates into coronary artery walls, where they then accumulate under coronary artery walls, causing atherosclerosis[27]. Figures 2(a) and 2(b) are schematics of LDL and ox-LDL, and the detailed components are described in Supplementary Materials.

2.2. Ox-LDL ELISA

The ox-LDL ELISA reagent kit (48T) was purchased from Shanghai Enzyme-linked Biotechnology Co., Ltd. (Shanghai, China). As shown in Fig. 3(a), 48 well microplates had been precoated with captured ox-LDL antibodies. Then, 100 μL of ox-LDL without illumination and ox-LDL after 40 min illumination were added into the wells, respectively. Meanwhile, one negative sample was included in each run as a control. Then, 100 μL of the enzyme-conjugated antibody was added into each

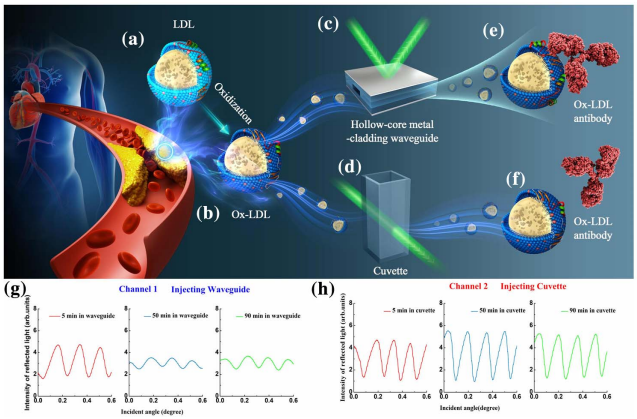

Fig. 2. Variation of ox-LDL in different light fields. (a) and (b) Structures of LDL and ox-LDL, respectively. Meanwhile, the detailed components are described in Supplementary Materials. (c) HCMW 3D schematic diagram. (d) Quartz cuvette. (e) The ox-LDL, which is illuminated in the HCMW. (f) The ox-LDL, which is illuminated in the cuvette. (g) The experimental reflection spectra for ox-LDL with different time exposures to the laser in the HCMW. (h) The experimental reflection spectra for ox-LDL with different time exposures to the laser in the cuvette.

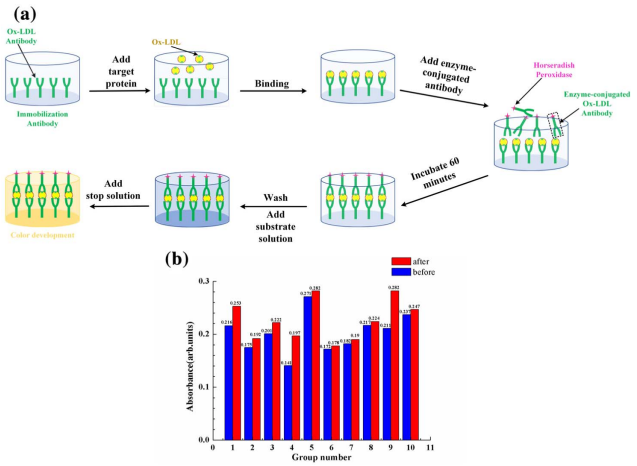

Fig. 3. ELISA experiment of ox-LDL after laser illumination. (a) Schematic illustration of ELISA experiment. (b) Optical density comparison of unilluminated ox-LDL and 40 min illuminated ox-LDL in the HCMW, respectively.

well. After incubating at 37°C for 1 h, the plate was washed five times, and the substrate was added (100 μL/well). The plate was intubated in dark at 37°C for 15 min again. The color reaction was stopped by adding 100 μL/well of stopping solution. Color intensity was measured by using a microplate reader with a 450 nm filter. The optic density (OD) values of the test samples were "blank corrected" by subtracting the OD value of the negative control. The ELISA experiments were carried out 10 times. The microplate reader ARM-100 was purchased from Hangzhou Allsheng Instruments Co., Ltd. (Hangzhou, China). The 450 nm filter was chosen.

2.3. NMR, micro-IR, and circular dichroism

The 1H nuclear magnetic resonance (NMR) spectra were recorded on a Bruker Avance Neo 700 spectrometer (700 MHz, Bruker, Rheinstetten, Germany). The spectra were recorded with the following acquisition parameters: temperature, 298 K; sweep width, 14,705.883 Hz, frequency of observing channel, 700.23 MHz; acquisition time, 1.114112 s; relaxation delay, d_1=2 s. All NMR data were processed and analyzed using the Bruker software TopSpin 4.1 (Bruker, Rheinstetten, Germany), and linewidth broadening (LB) was set to 0.3 Hz.

Before recording micro-infrared (IR) spectra, the sample was freeze-dried[28] in freeze-dried powder using freeze dryer Scientz-10 N/A (Ningbo Scientz Technology, Ningbo, China). Ox-LDL (30 μL, 2.2 mg/mL) that was both illuminated and unilluminated was contained in vials, respectively. The samples were freeze dried for 24 h at −58°C. The vacuum degree was set to 10 Pa. Micro-IR spectra were recorded on a Thermo Scientific Nicolet iN 10 micro-IR spectrometer (Thermo Fisher Scientific, MA, USA). The measurement range was set to 700–4000 nm.

Circular dichroism (CD) spectra were recorded on a Jasco J-1500 CD spectrometer (Jasco Corporation, Tokyo, Japan). Diluent 20 μL ox-LDL (2.2 mg/mL) was both illuminated and unilluminated with PBS (pH 7.4) to a concentration of 88 μg/mL. The illuminated and unilluminated ox-LDL samples were injected in micro cuvettes, respectively. The measurement range was set to 195–350 nm, the cell length to 10 nm, the data pitch to 0.5 nm, scanning speed to 50 nm/min, and bandwidth to 2 nm. The calculation of the simulation curves and analysis of secondary structures were supported by Spectra Manager II software (Jasco Corporation, Tokyo, Japan).

3. Results

3.1. Ox-LDL illuminated in HCMW and cuvette

Ox-LDL was injected into the HCMW and cuvette by using electronically controlled micro-syringe channel 1 and channel 2, respectively, as shown in Figs. 2(c)–2(f). The 532 nm CW laser (30 mW) was used to illuminate ox-LDL in the HCMW and cuvette. The intensity of reflected light of the HCMW filled with the ox-LDL solution was recorded by a photoelectric detector during the irradiation time. The curve of reflectivity measured from the HCMW tended to be flat after 45 min of laser beam illumination and achieved dynamic equilibrium in the same interval of reflectivity after another 40 min irradiation by the same laser beam, as shown in Fig. 2(g). Then, ox-LDL injected into the cuvette was illuminated by the same laser beam, and the illuminated ox-LDL in the cuvette was transferred into the HCMW to measure the intensity of reflected light. The measured reflectivity curves of the HCMWs, which were filled with 5 min (red), 45 min (blue), and 90 min illuminated ox-LDL (green) are presented in Fig. 2(h), respectively, which show little change. Compared with HCMW experimental data, the variation of reflectivity implied the structure of ox-LDL illuminated in HCMW changed after the laser irradiation.

3.2. Ox-LDL ELISA experiment

OD values represent the ox-LDL binding rate of ox-LDL antibody. A microplate reader was used to measure the OD values of both illuminated ox-LDL and unilluminated ox-LDL. OD values of ox-LDL without illumination and after 40 min illumination are presented in Fig. 3(b). All 10 times ELISA experiment results demonstrate that the OD value of the illuminated ox-LDL well is higher than without being illuminated in the same run. The average OD value of unilluminated ox-LDL wells is 0.2023, the average OD value of 40 min illuminated ox-LDL wells is 0.2267, while the value of 40 min illuminated ox-LDL wells increases 12.15% on average, as shown in Table 1. The results of the ELISA experiment indicate that the illuminated ox-LDL in the HCMW can increase the binding rate of ox-LDL and antibodies.

3.3. Comparison of different experiment parameters

Some parameters may influence the experiment results, the wavelength of the laser, the power of the beam, and the time of irradiation, for instance. Therefore, we compared the results with different irradiation parameters in Fig. 4. As shown in Fig. 4(a), the reflectivity spectra of different irradiation times are presented. The results demonstrate that the slope of measured ATR curves of incident light becomes smaller and tends to oscillate in a small range around a value during the first 30 min of laser beam irradiation (CW, 532 nm, 30 mW). Eventually, the ATR keeps dynamic equilibrium and oscillates in the same interval. As shown in Fig. 4(b), the variation of ATR peak ΔR, which represents the maximum value of one ATR peak minus the minimum ($\Delta R = R_{\max} - R_{\min}$), quickly declines in the first 30 min, and then stays around the same value in the next 60 min. It illustrates that the change of the ox-LDL secondary structure caused by irradiation in the HCMW is irreversible, and the new structure is stable. By comparing Figs. 4(c) and 4(d), the ATR peak variation rates and final stable intervals are different with the different irradiation power. In the first 20 min, the ATR curves tend to flatten with 50 mW incident light irradiation, and 5 mW incident light makes ATR change to small values. During the next 30 min, the ATR curves keep flat with 5 mW and 50 mW incident light irradiation, respectively. But, the final states of ATR are different, the 50 mW final interval of ATR is wider than the 5 mW result, and the 50 mW average reflectivity is lower than the 5 mW result. Finally, the different laser wavelengths are compared, as shown in Figs. 4(e) and 4(f). The variation rate of ATR with the laser wavelength of 473 nm irradiation is higher than at 532 nm, and the variation trends of ATR are almost identical under the 473 nm and 532 nm incident light illumination. Thus, comparing the experiment results with different parameters, the secondary structure of ox-LDL is changed by photocatalysis, and we provide a more detailed result difference caused by incident light wavelength, irradiation time, and laser power, which might be a reference in therapy.

Table 1. Experiment Data of ox-LDL ELISA, Both Exposed and Unexposed.

Group No.	Before	After	Rate of Increase (%)
1	0.216	0.253	17.20
2	0.175	0.192	9.70
3	0.201	0.222	10.40
4	0.141	0.197	39.70
5	0.271	0.282	4.10
6	0.172	0.178	3.40
7	0.182	0.190	4.40
8	0.217	0.224	3.20
9	0.211	0.282	25.20
10	0.237	0.247	4.20
Average	0.2023	0.2267	12.15

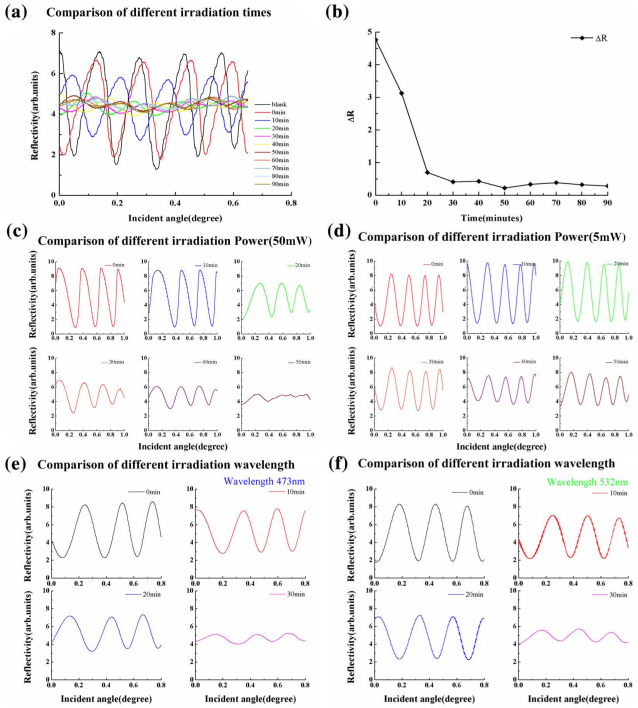

Fig. 4. Comparison of different experiment parameters. (a) The measured reflection spectra of the HCMW filled with different laser continuous irradiation time ox-LDL. (b) Image of ΔR with different laser irradiation time. (c) and (d) The measured reflection spectra of the HCMW filled with ox-LDL under the irradiation of 5 mW and 50 mW laser beams, respectively. (e) and (f) The measured reflection spectra of the HCMW filled with ox-LDL illuminated by 473 nm and 532 nm lasers, respectively.

4. Discussion

4.1. Ox-LDL change

To confirm the cause of binding rate increment of the ox-LDL antibody and 40 min illuminated ox-LDL, the 1H NMR spectra

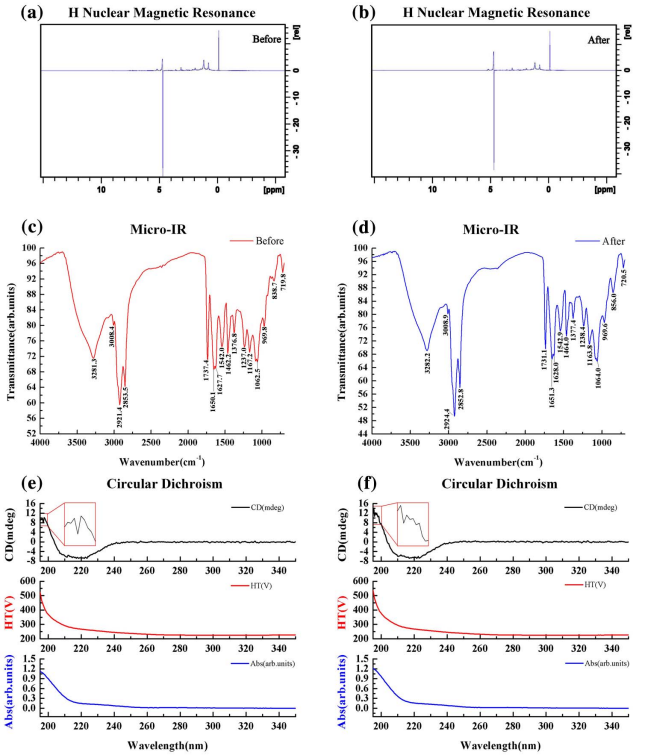

Fig. 5. Analysis of ox-LDL structures variation after laser irradiation. (a) and (b) 1H NMR spectra of ox-LDL before laser irradiation and after 40 min irradiation in the HCMW, respectively. (c) and (d) Micro-IR spectra of ox-LDL before laser irradiation and after 40 min illumination in the HCMW, respectively. (e) and (f) Circular dichroism (CD) spectra of both states of ox-LDL in the HCMW, respectively: CD (black), HT (red), and absorption of solution (blue).

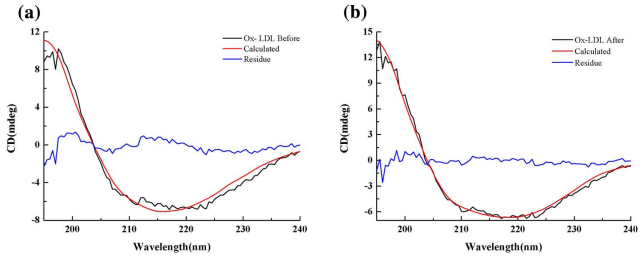

Fig. 6. (a) and (b) Experimental CD spectra (black), software simulation curves (red), and the difference between the measured CD spectra and software simulation curves (blue).

were measured as shown in Figs. 5(a) and 5(b). In terms of the position of peaks and ratio of peak intensity in two spectra, the primary structures of unilluminated ox-LDL and 40 min illuminated ox-LDL are not different. Likewise, the measured micro-IR spectra indicate the same results as the NMR spectra. As shown in Figs. 5(c) and 5(d), the peak positions and peak ratios in the two spectra are nearly the same, which implies that the organo-functional groups of unilluminated and 40 min illuminated ox-LDL are not different. According to NMR and micro-IR spectra, the primary structure of ox-LDL is not changed under the laser beam illumination in the HCMW. Therefore, the CD spectra were recorded to detect the change of ox-LDL's secondary structures. CD records the absorption intensity difference of left circularly polarized light and right circularly polarized light[29]; thus, the changes of spatial structure can be detected sensitively. As presented in Figs. 5(e) and 5(f), high tension (HT) is voltage applied on the photomultiplier tube (PMT) detector to amplify the detector's sensitivity, and Abs is the absorption of samples. The CD value of unilluminated ox-LDL is obviously smaller than that of 40 min illuminated ox-LDL at 195–200 nm, which is the characterized range of protein's CD value[29]. Hence, the secondary structures of ox-LDL lipoprotein changed after 40 min of laser illumination in the HCMW, as shown in Fig. 5.

Based on the software simulation and analysis, the content ratios of α-helix, β-sheet, and random structure of ox-LDL before irradiation are 4.3%, 65.3%, and 30.1% (RMS value 12.823), respectively, while the content ratios of α-helix, β-sheet, and random structure of ox-LDL after 40 min illumination (CW, 532 nm, 30 mW) in HCMW are 33.3%, 66.7%, and 0 (RMS value 8.257), respectively. By comparison of the above results, the increase of the α-helix content ratio is considerable, and the random structure content ratio is decreased, as shown in Fig. 6 and Supplementary Materials. The analysis results well explain that the combination rate of 40 min illuminated ox-LDL and ox-LDL antibody is increased. According to CD records, the content ratios of α-helix, β-sheet, and random structure of ox-LDL have changed in the HCMW.

4.2. Summary

In this work, we report a photocatalysis experiment reacting in the HCMW, which changed the secondary structures of ox-LDL. The HCMW provides a strong electromagnetic field, which can support the reactions while the cuvette cannot. According to the CD spectra, the significant content ratio variations of α-helix and β-sheet in ox-LDL before and after irradiation were confirmed, which lead to the binding rate of ox-LDL and ox-LDL antibody increasing. We also explored the impact on experiment results with different irradiation parameters; higher irradiation laser power and shorter irradiation laser wavelength can improve reaction speed, speeding up the change of ox-LDL's secondary structures. Our findings may offer a new method to remove ox-LDL *in vivo*, realizing non-invasive treatment of cardiovascular disease and improving a patient's quality of life.

Acknowledgement

This work was supported by the National Key R&D Program of China (No. 2018YFA0306301), the National Natural Science Foundation of China (NSFC) (Nos. 11734011, 11764020, and 12104298), the China Postdoctoral Science Foundation (Nos. 2020M681275 and 2021T140452), and the Foundation

for Shanghai Municipal Science and Technology Major Project (No. 2019SHZDZX01-ZX06).

References

1. J. Sanz and Z. Fayad, "Imaging of atherosclerotic cardiovascular disease," Nature **451**, 953 (2008).
2. J. L. Aldons, "Atherosclerosis," Nature **407**, 233 (2000).
3. P. Libby, P. Ridker, and G. Hansson, "Progress and challenges in translating the biology of atherosclerosis," Nature **473**, 317 (2011).
4. S. Tatsuya, K. Noriaki, A. Takuma, M. Hideaki, H. Hajime, A. Yuichi, T. Takeshi, M. Soichi, K. Yoshimoto, K. Toru, and M. Tomoh, "An endothelial receptor for oxidized low-density lipoprotein," Nature **386**, 73 (1997).
5. S. Parthasarathy, A. Raghavamenon, M. O. Garelnabi, and N. Santanam, "Oxidized low-density lipoprotein," Methods Mol. Biol. **610**, 403 (2010).
6. M. Tamminen, G. Mottino, J. Qiao, J. Breslow, and J. Frank, "Ultrastructure of early lipid accumulation in ApoE-deficient mice," Arterioscler. Thromb. Vasc. Biol. **19**, 847 (1999).
7. K. Nakajima, T. Nakano, and A. Tanaka, "The oxidative modification hypothesis of atherosclerosis: the comparison of atherogenic effects on oxidized LDL and remnant lipoproteins in plasma," Clinica Chimica Acta **367**, 36 (2006).
8. M. Quinn, S. Parthasarathy, L. Fong, and D. Steinberg, "Oxidatively modified low density lipoproteins: a potential role in recruitment and retention of monocyte/macrophages during atherogenesis," Proc. Natl. Acad. Sci. U. S. A. **84**, 2995 (1987).
9. S. Mitra, A. Deshmukh, R. Sachdeva, J. Lu, and J. L. Mehta, "Oxidized low-density lipoprotein and atherosclerosis implications in antioxidant therapy," Am. J. Med. Sci. **342**, 135 (2011).
10. T. Andreja, I. Resanovic, S. Julijana, R. Djordje, A. M. Shaker, C. M. Desanka, J. Danimir, and R. I. Esma, "Oxidized low-density lipoprotein as a biomarker of cardiovascular diseases," Crit. Rev. Clin. Lab. Sci. **52**, 70 (2015).
11. S. Choi, R. Harkewicz, J. H. Lee, A. Boullier, F. Almazan, A. C. Li, J. L. Witztum, Y. S. Bae, and I. M. Yury, "Lipoprotein accumulation in macrophages via toll-like receptor-4-dependent fluid phase uptake," Circ. Res. **104**, 1355 (2009).
12. R. Carnevale, S. Bartimoccia, C. Nocella, D. S. Serena, L. Lorenzo, I. Giulio, L. Elisabetta, B. Valentina, D. B. Maria, D. M. Luigi, P. Pasquale, and V. Francesco, "LDL oxidation by platelets propagates platelet activation via an oxidative stress-mediated mechanism," Atherosclerosis **237**, 108 (2014).
13. G. Obermayer, T. Afonyushkin, and C. J. Binder, "Oxidized low-density lipoprotein in inflammation-driven thrombosis," J. Thromb. Haemost. **16**, 418 (2018).
14. S. A. Thorne, S. E. Abbot, P. G. Winyard, D. R. Blake, and P. G. Mills, "Extent of oxidative modification of low density lipoprotein determines the degree of cytotoxicity to human coronary artery cells," Heart **75**, 11 (1996).
15. H. Kataoka, N. Kume, S. Miyamoto, M. Minami, M. Morimoto, K. Hayashida, N. Hashimoto, and T. Kita, "Oxidized LDL modulates Bax/Bcl-2 through the lectinlike Ox-LDL receptor-1 in vascular smooth muscle cells," Arterioscler. Thromb. Vasc. Biol. **21**, 955 (2001).
16. F. Sigala, K. Athanassios, S. Paraskevi, F. Konstantinos, M. Sophia, K. I. Efstathios, G. G. Vassilis, and A. Ioanna, "Oxidized LDL in human carotid plaques is related to symptomatic carotid disease and lesion instability," J. Vasc. Surg. **52**, 704 (2010).
17. S. M. Marcovina, F. Crea, J. Davignon, J. C. Kaski, W. Koenig, U. Landmesser, P. L. Pieri, M. J. Schulz, L. J. Shaw, and J. Sobesky, "Biochemical and bioimaging markers for risk assessment and diagnosis in major cardiovascular diseases: a road to integration of complementary diagnostic tools," J. Intern. Med. **261**, 214 (2007).
18. H. Itabe and M. Ueda, "Measurement of plasma oxidized low-density lipoprotein and its clinical implications," J. Atheroscler. Thromb. **14**, 1 (2007).
19. A. Sato, Y. Yamazaki, and K. Ebina, "A method for in vitro measurement of oxidized low-density lipoprotein in blood, using its antibody, fluorescence-labeled heptapeptide and polyethylene glycol," J. Fluoresc. **27**, 1985 (2017).
20. A. Zinellu, S. Salvatore, G. Franca, L. Fiorenza, P. Valeria, M. P. Giovanni, T. Bruna, D. Luca, and C. Ciriaco, "Applications on the monitoring of oxidative modification of LDL by capillary electrophoresis: a comparison with spectrophotometer assay," Talanta **64**, 428 (2004).
21. J. Stocks and N. Miller, "Analysis of apolipoproteins and lipoproteins by capillary electrophoresis," Electrophoresis **20**, 2118 (1999).
22. H. Hinterwirth, G. Stübiger, W. Lindner, and M. Lämmerhofer, "Gold nanoparticle-conjugated anti-oxidized low-density lipoprotein antibodies for targeted lipidomics of oxidative stress biomarkers," Anal. Chem. **85**, 8376 (2013).
23. E. Haller, G. Stübiger, D. Lafitte, W. Lindner, and M. Lämmerhofer, "Chemical recognition of oxidation-specific epitopes in low-density lipoproteins by a nanoparticle based concept for trapping, enrichment, and liquid chromatography-tandem mass spectrometry analysis of oxidative stress biomarkers," Anal. Chem. **86**, 9954 (2014).
24. H. Dai, L. Yuan, C. Yin, Z. Cao, and X. Chen, "Direct visualizing the spin Hall effect of light via ultrahigh-order modes," Phys. Rev. Lett. **124**, 053902 (2020).
25. H. Li, Z. Cao, H. Lu, and Q. Shen, "Free-space coupling of a light beam into a symmetrical metal-cladding optical waveguide," Appl. Phys. Lett. **83**, 2757 (2003).
26. C. Yin, X. Kan, K. Guo, T. Wang, J. Xu, Q. Han, J. Wu, and Z. Cao, "Highly twisted M-line of a vortex beam due to the coupling of ultrahigh-order modes," Chin. Opt. Lett. **19**, 071403 (2021).
27. G. Hansson, "Mechanisms of disease-inflammation, atherosclerosis, and coronary artery disease," N. Engl. J. Med. **352**, 1685 (2005).
28. A. Halil and P. Bahar, "Effect of purification, dehydration, and coagulation processes on the optical parameters of biological tissues," Chin. Opt. Lett. **19**, 011701 (2021).
29. Y. H. Chen, J. T. Yang, and K. H. Chau, "Determination of the helix and β form of proteins in aqueous solution by circular dichroism," Biochemistry **13**, 3350 (1974).